

Critical behavior of Ising model by preparing thermal state on quantum computer

Xiaoyang Wang^{1,2,3,*}, Xu Feng^{1,2,3}, Tobias Hartung⁴, Karl Jansen⁵, and Paolo Stornati⁶

¹*School of Physics, Peking University, Beijing 100871, China*

²*Collaborative Innovation Center of Quantum Matter, Beijing 100871, China*

³*Center for High Energy Physics, Peking University, Beijing 100871, China*

⁴*Northeastern University London, Devon House, St Katharine Docks, London, E1W 1LP, United Kingdom*

⁵*NIC, DESY Zeuthen, Platanenallee 6, 15738 Zeuthen, Germany*

⁶*ICFO-Institut de Ciències Fotoniques, The Barcelona Institute of Science and Technology, Av. Carl Friedrich Gauss 3, 08860 Castelldefels (Barcelona), Spain*

(Dated: September 7, 2023)

We simulate the critical behavior of the Ising model utilizing a thermal state prepared using quantum computing techniques. The preparation of the thermal state is based on the variational quantum imaginary time evolution (QITE) algorithm. The initial state of QITE is prepared as a classical product state, and we propose a systematic method to design the variational ansatz for QITE. We calculate the specific heat and susceptibility of the long-range interacting Ising model and observe indications of the Ising criticality on a small lattice size. We find the results derived by the quantum algorithm are well consistent with the ones from exact diagonalization, both in the neighborhood of the critical temperature and the low-temperature region.

I. INTRODUCTION

With the development of quantum devices and quantum algorithms, it is possible to solve problems on quantum computers that are hard for classical ones. Quantum computers have already been successfully implemented in many fields, including quantum chemistry, condensed matter physics and lattice field theory, see references [1–7] as some examples. With the growing number of qubits and improved fidelities of quantum devices, more realistic physical models can be tackled, and the potential of quantum computers can be explored. As an example of application, in this article, we prepare the thermal state of the Ising model with a quantum algorithm at various temperatures, including points close to the critical temperature and the low-temperature region. To demonstrate the feasibility of our approach, we compare the quantum simulation results of the chosen physical quantities with the results from classical simulations.

Numerous algorithms have been proposed to enable a quantum computer to prepare a thermal state. These include the quantum thermal dynamic method, where the target system is coupled with a bath at equilibrium [8], variational quantum algorithm based on the thermofield double state [9, 10], as well as many quantum imaginary time evolution (QITE) algorithms such as the one utilizing Hubbard-Stratonovich transformation [11], QITE based on variational ansatz (QITE-ansatz) [12], QITE based on measurement (QITE-measure) [13] and QITE by performing coordinatewise optimization [14]. The scope of our research is to focus on the usage of noisy intermediate-scale quantum (NISQ) devices [15, 16]. Given the presence of quantum noise, it is necessary to minimize the depth of the quantum circuits. We utilize

the QITE-ansatz algorithm to generate thermal states in our research, as it has a relatively shallower circuit depth in comparison to other algorithms mentioned previously. In QITE-ansatz algorithm, the imaginary time evolution is carried out on a prior parameterized quantum circuit, and the parameters are evolved variationally. Thus, the parameterized quantum circuit is usually called variational ansatz. The variational ansatz is designed for ground state preparation in most references utilizing QITE-ansatz, such as [12, 17, 18]. Here, for thermal state preparation, we propose to construct a variational ansatz converted from quantum circuits utilized in QITE-measure [13]. The circuit in QITE-measure can also carry out imaginary time evolution, but the circuit depth is quite large. The circuit depth can be much reduced by converting the circuit into a variational ansatz. For example, when simulating the Ising model, the quantum circuits in QITE-measure have ~ 100 layers, while the variational ansatz circuits used in this work have less than 10 layers.

In this article, we study the long-range interacting Ising model. Long-range interaction between spins is introduced naturally in trapped-ion spin systems [19], and its dynamics can be simulated utilizing quantum simulation algorithms. The long-range interaction also leads to interesting physics such as confinement [20] and meson scattering [21]. Meanwhile, the long-range interaction leads to effective dimensions that impact the system's critical behavior. Here, we calculate the specific heat of the long-range interacting Ising model near the critical point and in the low-temperature region.

This article is organized as follows. In section II, we introduce the long-range interacting Ising model and the measurement method of relevant physical quantities on a quantum computer. In section III, we discuss the process of thermal state preparation using QITE-ansatz algorithm in detail, especially the method of variational ansatz design. In section IV, we present the numerical

* zzwxy@pku.edu.cn

results and discuss the observed indications of the criticality. Finally, in section V, we summarize the techniques used in this article and discuss the possible extension for further works.

II. LONG-RANGE INTERACTING ISING MODEL

We consider the $D = 2$ dimensional Ising model on a square lattice Λ with long-range interactions. The Hamiltonian reads

$$H = - \sum_{i>j \in \Lambda} \frac{J}{r_{ij}^\alpha} Z_i Z_j - h \sum_i Z_i, \quad (1)$$

where Z_i is the Pauli- Z operator on the i th spin. J is the bare coupling strength, and α denotes the range of the interaction. h denotes the strength of the longitudinal external field. The distance r_{ij} is defined by the Manhattan distance under periodic boundary condition(PBC): Assuming the position of spin i on the square lattice is represented by integer vector $\vec{r}^i = (r_1^i, \dots, r_D^i)$ and the volume of the lattice is $|\Lambda| = N_1 \times \dots \times N_D$, then

$$r_{ij} = \sum_{d=1}^D \min(|r_d^i - r_d^j|, N_d - |r_d^i - r_d^j|). \quad (2)$$

This Hamiltonian is a generalization of the interaction part of the Hamiltonian introduced in reference [20]. It reduces to the original nearest-neighbor Ising model (NNIM) in the limit $\alpha \rightarrow \infty$. Because in the limit $\alpha \rightarrow \infty$, all the long-range couplings J/r_{ij}^α with $r_{ij} > 1$ vanish, except for nearest-neighbor ones with $r_{ij} = 1$.

The state of the Ising system at a finite temperature is described by the density operator. Its equilibrium state is the Gibbs state of which the density operator reads

$$\rho = \frac{1}{Z_\beta} e^{-\beta H}, \quad Z_\beta \equiv \text{tr}(e^{-\beta H}). \quad (3)$$

Here β is the inverse temperature $\beta \equiv 1/(k_B T)$ and we define $K \equiv J\beta$ for later convenience. For an arbitrary observable O , its expectation value of the thermal state is given by

$$\langle O \rangle \equiv \text{tr}(\rho O). \quad (4)$$

This article targets the case where the expectation values are evaluated for different K and a zero external field $h = 0$.

Now we exhibit observables to compute the Ising model's specific heat and susceptibility. Analyzing these measures allows us to examine the critical behavior of the Ising model. The specific heat is defined by the changing rate of the internal energy in a unit volume when varying the temperature T . It can be evaluated by the energy-fluctuation relation:

$$C_v \equiv \frac{1}{|\Lambda|} \frac{\partial \langle H \rangle}{\partial T} = \frac{1}{|\Lambda| T^2} [\langle H^2 \rangle - \langle H \rangle^2], \quad (5)$$

where the last expression can be derived by taking the Gibbs state Eq. (3) to evaluate the expectation values.

Similarly, the susceptibility is defined by the changing rate of the magnetization in a unit volume with respect to the external field strength h (evaluated at $h = 0$). The total magnetization is given by

$$\langle M \rangle \equiv \langle Z_{tot} \rangle, \quad (6)$$

where $Z_{tot} \equiv \sum_i Z_i$, i.e., the sum of all the spins in the lattice. Then the susceptibility can be evaluated according to the susceptibility-fluctuation relation

$$\chi \equiv \frac{1}{|\Lambda|} \left. \frac{\partial \langle M \rangle}{\partial h} \right|_{h=0} = \frac{1}{|\Lambda| T} [\langle Z_{tot}^2 \rangle - \langle Z_{tot} \rangle^2]. \quad (7)$$

In summary, evaluating the specific heat and susceptibility is equivalent to calculating the expectation values of the corresponding operators. The operators to be measured include

$$H^2, H, Z_{tot}^2, Z_{tot} \quad (8)$$

which can all be reduced to linear combinations of Pauli operators. To evaluate the expectation values of the above operators on quantum computers, we can generate the thermal state utilizing a quantum algorithm and then evaluate the expectation values of the Pauli operators. Notice that for the above operators, the elementary Pauli operators can be written as products of Pauli- Z operators, so they commute and can be measured simultaneously on the quantum computer. Combined with the fact that the Hamiltonian in Eq. (1) consists of only Pauli- Z operators, we can simplify the initial state to be evolved on quantum computer. It enables us to simulate the system on a larger lattice. For general models, such as the Ising model with a transversal field, the simplification does not hold. More details can be found in section (III A).

III. THERMAL STATE PREPARATION WITH QUANTUM IMAGINARY TIME EVOLUTION

One can use the quantum imaginary time evolution(QITE) algorithm to prepare a thermal state [22], as demonstrated in previous studies [12, 13]. This section provides an explanation of the QITE-ansatz algorithm. QITE-ansatz algorithm is designed to evolve an N_q -qubit quantum state $|\psi(0)\rangle$ to

$$|\psi(\tau)\rangle = \frac{e^{-\tau H} |\psi(0)\rangle}{\sqrt{\langle \psi(0) | e^{-2\tau H} | \psi(0) \rangle}}, \quad (9)$$

where τ is a real number denoting imaginary time. The denominator is a normalization factor to guarantee the evolution's unitarity. Assuming we have the quantum circuit to carry out the unitary evolution, then by choosing the initial state to be the maximally mixed state (defined

as the density operator) $|\psi(0)\rangle\langle\psi(0)| = \mathbf{I}/\mathbf{d}$ [23] (\mathbf{I} is the identity operator of the $\mathbf{d} \equiv 2^{N_q}$ dimensional Hilbert space), one finds the final state is the thermal state with inverse temperature $\beta = 2\tau$

$$|\psi(\tau)\rangle\langle\psi(\tau)| = \frac{1}{Z_{2\tau}} e^{-2\tau H}, \quad Z_{2\tau} \equiv \text{tr}(e^{-2\tau H}). \quad (10)$$

The QITE-ansatz algorithm was proposed in references [12, 24]. This technique is originally used to project out the ground state of the Hamiltonian according to Eq. (9). It has been successfully implemented in the field of quantum chemistry, quantum field theory and machine learning, see e.g. [1, 17, 18].

Following [24], we first review the QITE-ansatz algorithm within the density operator formalism. The density operator of Eq. (9) reads

$$\rho(\tau) = \frac{e^{-\tau H} |\psi(0)\rangle\langle\psi(0)| e^{-\tau H}}{\langle\psi(0)| e^{-2\tau H} |\psi(0)\rangle}. \quad (11)$$

The mathematical description of a quantum state with the density operator is equivalent to that with the pure state. In particular, the expectation values of any observable O coincide

$$\text{tr}(\rho(\tau)O) = \langle\psi(\tau)| O |\psi(\tau)\rangle. \quad (12)$$

The imaginary time evolution of the density operator follows the von-Neumann equation [24]

$$\frac{d\rho(\tau)}{d\tau} = \mathcal{L}[\rho(\tau)], \quad (13)$$

where \mathcal{L} is the Liouville operator defined by $\mathcal{L}(\rho) = -\{H, \rho\} + 2\text{tr}(\rho H)\rho$ with anti-commutator $\{H, \rho\} = H\rho + \rho H$. As the Hilbert space of the whole N_q qubits is hard to be explored by a quantum circuit, we utilize a density operator $\hat{\rho}(\tau) = |\phi(\tau)\rangle\langle\phi(\tau)|$ to approximate the target density $\rho(\tau)$. The approximation $\hat{\rho}(\tau)$ satisfies the following requirements: (1) It has the same initial state $\hat{\rho}(0) = \rho(0) = |\psi(0)\rangle\langle\psi(0)|$. (2) The evolution of $\hat{\rho}(\tau)$ approximately satisfies the von-Neumann equation $d\hat{\rho}(\tau)/d\tau - \mathcal{L}[\hat{\rho}(\tau)] = 0$.

The approximation $\hat{\rho}(\tau)$ is generated with a variational ansatz $|\phi(\vec{\theta}(\tau))\rangle = U(\vec{\theta}(\tau))|\psi(0)\rangle$, where $\vec{\theta}$ is a real variational parameter vector with N components. $U(\vec{\theta}) = U_N(\theta_N) \dots U_1(\theta_1)$ is a series of parameterised unitary quantum gates. According to the first requirement mentioned above, $U(\vec{\theta}(0))$ should be the identity operator \mathbf{I} . With the variational ansatz, the evolution of the quantum state is converted to the evolution of the variational parameters $\vec{\theta}$. However, as the variational ansatz cannot explore the whole Hilbert space, $|\phi(\vec{\theta}(\tau))\rangle$ can not fulfill the von-Neumann equation exactly. Instead, we demand that the von-Neumann equation is fulfilled sufficiently well according to the second requirement. The violation of the von-Neumann equation is

measured by the McLachlan distance L^2 , which is defined by

$$L^2 \equiv \left\| \frac{d\hat{\rho}(\tau)}{d\tau} - \mathcal{L}[\hat{\rho}(\tau)] \right\|^2, \quad (14)$$

where $\|A\|^2 = \text{tr}(A^\dagger A)$ represents Frobenius norm. According to the differential chain rule, we have

$$L^2 = \left\| \sum_{\mu} \frac{\partial \hat{\rho}(\theta)}{\partial \theta_{\mu}} \dot{\theta}_{\mu} - \mathcal{L}(\hat{\rho}) \right\|^2. \quad (15)$$

So that the McLachlan distance is a quadratic function of the time derivatives of the variational parameters $\dot{\theta}_{\mu} \equiv \partial \theta_{\mu} / \partial \tau$. L^2 can be minimized with the variational principle, which leads to

$$\delta L^2 = 0 \Rightarrow \frac{\partial L^2}{\partial \dot{\theta}_{\mu}} = \sum_{\nu} M_{\mu\nu} \dot{\theta}_{\nu} - V_{\mu} = 0, \quad (16)$$

where

$$M_{\mu\nu} \equiv 2 \text{Re} \left[\frac{\partial \langle \phi(\vec{\theta}) |}{\partial \theta_{\mu}} \frac{\partial | \phi(\vec{\theta}) \rangle}{\partial \theta_{\nu}} \right], \quad (17)$$

$$V_{\mu} \equiv -2 \text{Re} \left[\frac{\partial \langle \phi(\vec{\theta}) |}{\partial \theta_{\mu}} H | \phi(\vec{\theta}) \rangle \right].$$

Here M is a $N \times N$ matrix while V is a N dimensional vector. Following [12, 25], one can construct some specific quantum circuits to measure M and V , which cost $\mathcal{O}(N^2)$ quantum device calls and one additional ancilla qubit.

After deriving M and V , we can construct the following linear equations

$$\sum_{\nu} M_{\mu\nu} \dot{\theta}_{\nu} = V_{\mu}. \quad (18)$$

Then one can solve for the time derivative of the variational parameters $\dot{\theta}_{\nu}|_{\tau=\tau_0}$ at a given imaginary time τ_0 , utilizing methods such as pseudo-inverse [12]. The variational parameters at the next time slice $\tau_0 + \delta\tau$ are given according to the Euler method

$$\vec{\theta}(\tau_0 + \delta\tau) \simeq \vec{\theta}(\tau_0) + \vec{\dot{\theta}}\delta\tau, \quad (19)$$

where $\dot{\theta}_{\nu} = \sum_{\mu} M_{\nu\mu}^{-1} V_{\mu}$.

The computational complexity of the QITE-ansatz grows polynomially with the number of variational parameters N . In each time slice, the time complexity of solving linear equations grows polynomially with N , while the matrix M and vector V can also be evaluated using quantum computers within polynomial time. Thus as long as N grows polynomially with the system size N_q , the time complexity of the QITE-ansatz grows polynomially with N_q and can be extended to large-scale quantum systems. The following subsections will introduce how to prepare the maximally mixed state and choose an appropriate variational ansatz.

A. Initial state preparation

Here we introduce how to prepare the initial state as the maximally mixed state \mathbf{I}/\mathbf{d} . Quantum circuits are suitable for generating pure states. We need some strategies to generate mixed states utilizing pure states. As discussed in [26], there are two strategies: ancilla pair state (APS) and classical product state (CPS). Both strategies can be used to prepare maximally mixed state \mathbf{I}/\mathbf{d} . However, preparing \mathbf{I}/\mathbf{d} with APS doubles the number of qubits to $2N_q$ [18]. It also introduces some complexities in variational ansatz design to evolve the pair state.

Instead, we can prepare the maximally mixed state via CPS, which reduces the required qubits to N_q . The maximally mixed state \mathbf{I}/\mathbf{d} describes that the probabilities of sampling every basis vector from a given orthogonal basis are the same, where each basis vector is a pure state. As the maximally mixed state is unitarily invariant $U(\mathbf{I}/\mathbf{d})U^{-1} = \mathbf{I}/\mathbf{d}$, the orthogonal basis can be chosen arbitrarily. To generate the thermal state, it is recommended in [26] to use a basis formed by classical product states, such as $\{|+\rangle, |-\rangle\}^{\otimes N_q}$, where $\{\cdot\}^{\otimes N_q}$ represents a set generated by the N_q times tensor product of each element in $\{\cdot\}$. For example,

$$\{|+\rangle, |-\rangle\}^{\otimes 2} = \{|++\rangle, |+-\rangle, |-+\rangle, |--\rangle\}. \quad (20)$$

Here $|+\rangle, |-\rangle$ represent the eigenvectors of the Pauli- X operator

$$X|+\rangle = |+\rangle, \quad X|-\rangle = -|-\rangle. \quad (21)$$

If we use the classical product state as the initial state, the thermal expectation value $\langle O \rangle$ can not be measured straightforwardly due to the normalization factor in Eq. (9). Assume that we take the orthogonal basis as $\{|i\rangle\}$. Evolving all basis vectors $|i\rangle$ for imaginary time τ , one gets the expectation values of an observable O , which read

$$\langle i(\tau) | O | i(\tau) \rangle = \frac{\langle i | e^{-\tau H} O e^{-\tau H} | i \rangle}{\langle i | e^{-2\tau H} | i \rangle}. \quad (22)$$

Usually, the denominators would be different for different basis vectors $|i\rangle$. To derive the thermal expectation value $\langle O \rangle$ in Eq. (4), we should multiply the above expectation values with coefficients $\{p_i\}$

$$\langle O \rangle = \sum_i p_i \langle i(\tau) | O | i(\tau) \rangle, \quad (23)$$

where p_i is defined by

$$p_i \equiv \frac{\langle i | e^{-2\tau H} | i \rangle}{Z_{2\tau}}. \quad (24)$$

Here $\{p_i\}$ can be treated as a probability distribution, as they are all positive and satisfy the normalization condition $\sum_i p_i = 1$. To evaluate the thermal expectation

value of the operator O , as mentioned in [13], we do not need to calculate all the $\{p_i\}$ (which would be impossible to calculate, as the number of p_i grows exponentially with the number of qubits). With the minimally entangled typical thermal state (METTS) algorithm proposed by Stoudenmire and White [27], one can sample $\{|i\rangle\}$ according to the distribution $\{p_i\}$. The thermal expectation value $\langle O \rangle$ is the average of the expectation of O with the time-evolved sampled vectors. In conclusion, though imaginary time evolution with CPS as initial states requires the number of qubits equal to the system size, one has to evolve different initial states $|i\rangle$ to acquire statistics. On the other hand, imaginary time evolution with APS as an initial state doubles the number of qubits while evolving only one initial state.

However, the situation gets simplified when we consider the classical Ising model and the observables in Eq. (8), which consist of Pauli- Z operators. The observables can be generally expressed as

$$O = \sum_m h_m \tilde{Z}_m. \quad (25)$$

Here \tilde{Z}_m represents the tensor product of Z operators at some sites and identity operators at the others, such as $\tilde{Z}_m = Z_{N_q-1} \dots I_1 Z_0$. In Appendix A, we prove that the thermal expectation value of O can be calculated according to

$$\langle O \rangle = \sum_m h_m \langle \tilde{+}(\tau) | \tilde{Z}_m | \tilde{+}(\tau) \rangle, \quad (26)$$

where $|\tilde{+}(\tau)\rangle$ is imaginary time evolved state according to Eq. (9). The state is initialized as $|\tilde{+}(0)\rangle = |\tilde{+}\rangle$, where $|\tilde{+}\rangle \equiv |+\rangle^{\otimes N_q}$ is the N_q -fold tensor product of $|+\rangle$ in Eq. (21). Thus for the Ising model, we only need to calculate the imaginary time evolution with the initial state $|\tilde{+}\rangle$.

In this work, we use $|\tilde{+}\rangle$ as the initial state to present our results. For general models, such as the Ising model with a transversal field, the above simplification does not hold. We need to sample the classical product states using the METTS algorithm or utilize the ancilla pair state.

B. Variational ansatz design

Choosing a proper variational ansatz is a cornerstone for the success of the QITE-ansatz algorithm [16]. In most literature on QITE-ansatz, the variational ansatz is designed to prepare the ground state of a Hamiltonian, and it is suitable to evolve some specific initial states, such as the unitary coupled cluster ansatz evolving Hartree-Fock states [1]. Focusing on thermal state preparation and the initial state introduced in the previous section, we propose to construct a variational ansatz

converted from quantum circuits utilized in the QITE-measure algorithm proposed by Motta et. al. [13].

We briefly introduce how to construct the quantum circuits used in the QITE-measure algorithm. The goal of QITE-measure is also evolving an initial state $|\psi(0)\rangle$ according to Eq. (9). Consider evolving the state $|\psi(\tau_0)\rangle$ for a small time slice $\Delta\tau$

$$|\psi(\tau_0 + \Delta\tau)\rangle = \frac{e^{-\Delta\tau H} |\psi(\tau_0)\rangle}{\sqrt{\langle\psi(\tau_0)| e^{-2\Delta\tau H} |\psi(\tau_0)\rangle}}. \quad (27)$$

As this transformation is unitary, we can always find a Hermitian operator $\hat{A}(\tau_0)$ such that

$$|\psi(\tau_0 + \Delta\tau)\rangle = e^{-i\Delta\tau \hat{A}(\tau_0)} |\psi(\tau_0)\rangle, \quad (28)$$

and $\hat{A}(\tau_0)$ can be expanded in a complete Pauli basis

$$\hat{A}(\tau_0) = \sum_{i_1 \dots i_{N_q}} a_{i_1 \dots i_{N_q}}^{(\tau_0)} \sigma_{i_1} \dots \sigma_{i_{N_q}} \equiv \sum_I a_I^{(\tau_0)} \tilde{\sigma}_I, \quad (29)$$

where the expansion coefficients $a_{i_1 \dots i_{N_q}}^{(\tau_0)}$ are real due to the Hermiticity of $\hat{A}(\tau_0)$, and $\sigma_{i_j} = I, X, Y, Z$ corresponding to $i_j = 0, 1, 2, 3$ is the single-qubit Pauli operator on the site j , and we call the tensor product of the single-qubit Pauli operator, $\tilde{\sigma}_I$ as Pauli string. For this reason, the single-qubit Pauli operator is sometimes called Pauli letter [28]. For each imaginary time τ_0 , one can calculate all the expansion coefficients $a_I^{(\tau_0)}$ by evaluating the expectation values of some observables with respect to the quantum state $|\psi(\tau_0)\rangle$. The observables are the composition of Pauli strings and the Hamiltonian (See more details in [13]). Notice that the transformation in Eq. (28) can be approximated by

$$e^{-i\Delta\tau \sum_I a_I^{(\tau_0)} \tilde{\sigma}_I} = \prod_I e^{-i\Delta\tau a_I^{(\tau_0)} \tilde{\sigma}_I} + \mathcal{O}(\Delta\tau^2), \quad (30)$$

where the product consists of several Pauli exponentials which have the form $e^{-i\theta \tilde{\sigma}_I}$, and the Pauli exponential can be realized with quantum gates in a standard way [29]. Thus, the whole quantum circuit used in the QITE-measure can be constructed using several Pauli exponentials for each time slice. In the last time slice, the circuit depth is proportional to the final imaginary time τ .

Notice that if a system has N_q qubits, the total number of Pauli strings on these qubits is 4^{N_q} . Thus the number of Pauli exponentials required for evolving each time slice seems exponential as a function of system size according to Eq. (29). However, the situation gets simplified when the Hamiltonian H consists of some local interaction terms

$$H = \sum_m H_m, \quad (31)$$

where each H_m acts on a local set of qubits, and the number of H_m is polynomial as a function of system size. For

example, $H_m \propto Z_i Z_j$ and the number of H_m is $\mathcal{O}(N_q^2)$ in case of long-range interacting Ising model. Though the local terms H_m may not commute, the imaginary time evolution $e^{-\Delta\tau H}$ can be decomposed by

$$e^{-\Delta\tau H} = \prod_m e^{-\Delta\tau H_m} + \mathcal{O}(\Delta\tau^2). \quad (32)$$

Then the previous steps in QITE-measure can be implemented for each $e^{-\Delta\tau H_m}$. As shown in [13], when the Hamiltonian consists of local terms and the correlation length of the system is finite, the expansion in Eq. (29) for each H_m can be implemented with Pauli strings on a support constantly larger than the support of H_m (Support of a Pauli string is defined by the set of qubits on which the Pauli letters are not identity). The correlation length of a system is finite when its Hamiltonian is outside the critical region. Thus the support of the Pauli strings has no dependence on the system size, and the total number of Pauli exponentials $e^{-i\theta \tilde{\sigma}_I}$ is a polynomial function of the system size at least when the Hamiltonian is sufficiently far away from the critical point.

Compared with the QITE-ansatz, the precision of the QITE-measure is not limited by the variational ansatz. However, the circuit depth grows linearly with the evolution time τ . Thus this algorithm would be very sensitive to coherent or incoherent noise in real quantum devices and can only be applied to small spin systems [30].

Quantum circuits constructed in QITE-measure can be naturally converted into a variational ansatz with the following steps: (1) using all the necessary Pauli exponentials at one time slice as one layer of the variational ansatz; (2) sequentially repeating the layer several times in the quantum circuit; (3) converting all the expansion coefficients $a_I^{(\tau_0)}$ into undetermined parameters, which are initially zero and to be evolved according to the QITE-ansatz algorithm. Times of repetition for one layer is called the depth of the variational ansatz, also called the number of layers.

The behavior of this variational ansatz can be analyzed with the help of QITE-measure. Assuming we have the same quantum circuit layers for the variational ansatz in QITE-ansatz and the quantum circuits in QITE-measure. Because the states prepared in QITE-measure can all be explored by the variational ansatz, one can expect QITE-ansatz using this circuit to behave at least better than QITE-measure. The systematic error of the QITE-measure circuit is of the first-order Trotter type, i.e., error $\sim \mathcal{O}(\Delta\tau)$ [13]. By equalizing the longest circuit depth used in QITE-measure and the depth in variational ansatz, it can be deduced that in the worst case, the variational ansatz leads to an error of $\mathcal{O}(1/L)$, where L is the number of layers.

In the numerical simulations, we find that the circuit depth required in QITE-ansatz is much smaller than that required in the QITE-measure. For example, in our numerical simulation of the Ising model, if the imaginary time of the final state is $\tau = 0.5$, with step size

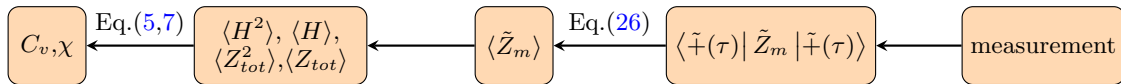


Figure 1. An illustration of the measurement process. The specific heat C_v and susceptibility χ of Ising model can be calculated by the measurement in computational basis on quantum computers.

$\Delta\tau = 0.002$, QITE-measure requires the number of layers $\tau/\Delta\tau = 250$. In contrast, to reach a sufficiently good precision using the variational ansatz, we find the number of layers required is at most $L = N_d$ for the 2-D nearest neighbor Ising model where N_d is the side length of the Ising lattice system. More details on the number of circuit layers required are shown in Appendix B.

The variational ansatz can be simplified due to some special structures of the Hamiltonian and the initial state. In the numerical simulations, we notice that some of the variational parameters are always zero during the whole evolution, which corresponds to the same set of Pauli strings over all the layers. We call the Pauli string in this set *irrelevant*, and the other Pauli strings corresponding to non-zero variational parameters are *relevant*. As the irrelevant Pauli exponentials are identity, they can be removed a priori when constructing the variational ansatz. These irrelevant Pauli strings can be identified according to the symmetry and some special structures of the Hamiltonian and the initial state. For example, if all the entries in the Hamiltonian and the initial state are real, then the corresponding unitary operator $e^{-i\Delta\tau A}$ should also be real. Thus all Pauli strings with an even number of Pauli- Y letters are irrelevant.

We demonstrate the above construction of variational ansatz using an example of a two-qubit ($N_q = 2$) Ising system. There are $4^2 = 16$ Pauli strings on the two-qubit system. Assume we have an initial state $|++\rangle$ and the system Hamiltonian $H = -Z_1 Z_0$. Because all the entries in the Hamiltonian and the initial state are real, eliminating Pauli strings with an even number of Pauli- Y letters leaves 6 Pauli strings: $I_1 Y_0, X_1 Y_0, Y_1 I_0, Y_1 X_0, Z_1 Y_0, Y_1 Z_0$. Evolving one layer with these 6 Pauli strings using QITE-ansatz, we further find 4 Pauli strings are irrelevant. It leaves only two relevant Pauli strings for the imaginary time evolution

$$Z_1 Y_0, Y_1 Z_0. \quad (33)$$

One can verify that

$$e^{-\Delta\tau H} |++\rangle = e^{\Delta\tau Z_1 Z_0} |++\rangle \propto e^{-ia_1(0)Z_1 Y_0} e^{-ia_2(0)Y_1 Z_0} |++\rangle, \quad (34)$$

with expansion coefficients

$$a_1^{(0)} = a_2^{(0)} = \frac{1}{2} \tan^{-1}(\tanh \Delta\tau). \quad (35)$$

In the QITE-measure algorithm, to evolve the initial state to an arbitrary time τ , the quantum circuit is

shown in figure 2a. It has $\tau/\Delta\tau$ layers. The variational ansatz with L layers for the two-qubit Ising system is constructed as shown in figure 2b. In this circuit, $\{\theta_1, \theta'_1 \dots \theta_L, \theta'_L\}$ are all variational parameters, taking zero as initial values, and to be evolved according to the QITE-ansatz algorithm.

Algorithm 1 QITE-ansatz algorithm for Ising model

Construct ansatz $|\phi(\vec{\theta}(\tau))\rangle$ for the Ising Hamiltonian H .
 Initial inverse temperature $K = 2\tau \leftarrow 0$.
 Rotation angles $\vec{\theta}(0) \leftarrow \vec{0}$.
 Initial state $|\phi(\vec{0})\rangle \leftarrow |\tilde{\dagger}\rangle$
while $\tau \leq \tau_{\max}$ **do**
 Calculate specific heat and susceptibility by the measurement process in Figure 1.
 Calculate matrix M and vector V in Eq. (17)
 Update rotation angles: $\vec{\theta}(\tau + \delta\tau) \leftarrow \vec{\theta}(\tau) + \delta\tau \cdot M^{-1}V$.
 $\tau \leftarrow \tau + \delta\tau$
end while

IV. NUMERICAL RESULTS

In this section, we apply the previous variational ansatz design procedure to the long-range interacting Ising model, where we prepare CPS $|\tilde{\dagger}\rangle$ as the initial state. Equipped with the thermal state, we can calculate the specific heat C_v and susceptibility χ as a function of $K \equiv J\beta$. The measurement process for C_v and χ is shown schematically in Figure 1. The QITE-ansatz algorithm for Ising model is compactly shown in Algorithm 1. Our numerical simulations are carried out on the Qiskit noiseless statevector quantum simulator [31].

The initial state and variational ansatz are chosen as described in section III. To calculate the thermal expectation values of the Ising model, we only need to calculate the imaginary time evolution of the product state $|\tilde{\dagger}\rangle$. With the initial state, and for every local interaction term in Ising model $Z_i Z_j (\forall i, j \in \Lambda)$, we have the corresponding relevant Pauli strings

$$Z_i Y_j, Y_i Z_j. \quad (36)$$

Then we can construct the variational ansatz for the target Ising Hamiltonian, i.e., for finite α , since the lattice sites are all-to-all coupled with the $Z_i Z_j$ term, the Pauli exponentials gates $e^{-i\theta Z_i Y_j}$ and $e^{-i\theta Y_i Z_j}$ are added with

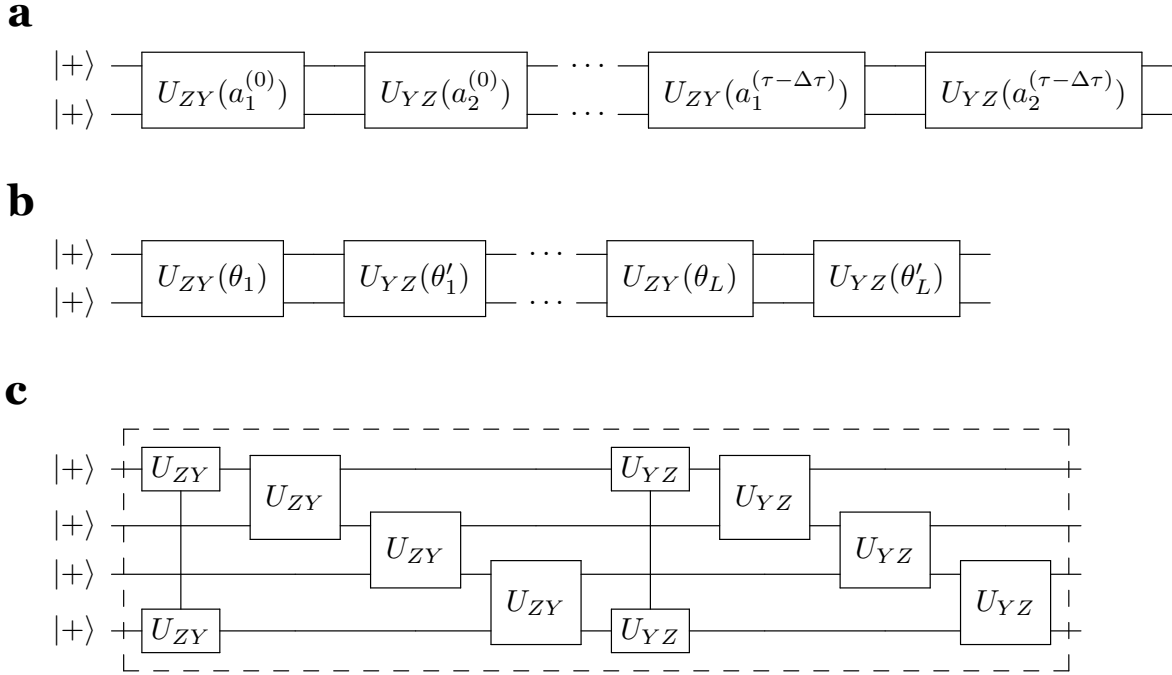


Figure 2. Example of circuits for the imaginary time evolution of Ising systems. The basic building blocks of the circuits are defined as $U_{ZY}(\theta) \equiv e^{-i\theta ZY}$, $U_{YZ}(\theta) \equiv e^{-i\theta YZ}$. (a) The quantum circuit in the QITE-measure algorithm to carry out the imaginary time evolution $e^{\tau ZZ} |++\rangle$. $\Delta\tau$ is the length of one time slice. (b) The variational ansatz converted from the QITE-measure circuit. L is the number of circuit layers, $\theta_i, \theta'_i, i \in [1, L]$ are free variational parameters. (c) The variational ansatz for nearest neighbor 1-D Ising chain under the periodic boundary condition. Each layer consists of one layer of ZY-Pauli exponentials and one layer of YZ-Pauli exponentials, as shown in the dashed box. The figure shows the case of one layer.

all-to-all connection. While for infinite α , only nearest-neighbor couplings are considered in the Hamiltonian. So the gates are added only between pairs of nearest neighbor sites. An example of a variational ansatz for nearest-neighbor Ising chain under periodic boundary conditions is shown in figure 2c. Each layer of the variational ansatz consists of one layer of ZY-Pauli exponentials and one layer of YZ-Pauli exponentials, as shown in the dashed box. The Pauli exponentials are ladder-arranged, to increase the correlation between sites that can be generated by the variational ansatz. In the figure, we show the case of layers $L = 1$. In the following numerical simulations, we use $L = 2$ if not specified otherwise.

We assume the imaginary time evolution of each local interaction term $e^{\tau Z_i Z_j}$ can be realized with the Pauli exponentials $e^{-i\theta Z_i Y_j} e^{-i\theta' Y_i Z_j}$, which have the same support of $Z_i Z_j$. These two Pauli exponentials are enough in the 2-qubit case as indicated by Eq. (34), but are not when the system size is large and when the system approaches the critical point, as explained in the previous section. It means that the expressivity of this variational ansatz is not sufficiently good to carry out the whole imaginary time evolution $e^{-\tau H}$. Limited expressivity leads to systematic errors, which will affect the numerical results.

First, we present the numerical results of the nearest-

neighbor Ising model (NNIM), i.e., taking the limit $\alpha \rightarrow \infty$ in Eq. (1). With the nearest-neighbor interaction, there are $N = 2D|\Lambda|L$ parameters in the variational ansatz. In two and three-dimensional NNIMs, there is a second-order phase transition in the infinite volume limit, where the critical points are $K_c = \ln(1 + \sqrt{2})/2 \approx 0.441$ [32] and 0.222 [33] for dimension $D = 2, 3$, respectively. The specific heat and susceptibility would hence diverge near the critical point in the infinite volume limit. Figure 3 shows the specific heat and susceptibility for various K values obtained via QITE-ansatz. The lattice size is $2 \times 2, 3 \times 3, 4 \times 4$ for the 2-D system, marked by triangular-down, circle and triangular-up, respectively, and $2 \times 2 \times 2, 3 \times 3 \times 2$ for the 3-D system, with results marked by triangular-down and circle respectively. In the evolution of the variational parameters, we use the Euler method with step length $\delta\tau = 0.002$ as in Eq. (19), which is chosen such that further shrinking the step length has no impact on the numerical results (We will take this step length also throughout the following simulations.). We see that the QITE results converge well with the results from exact diagonalization (ED) when the system size is small for both 2-D and 3-D systems. For 4×4 and $3 \times 3 \times 2$ lattices, the specific heat curves deviate from the ED curves near the critical point, which result from the limitation of the variational ansatz expressivity. The

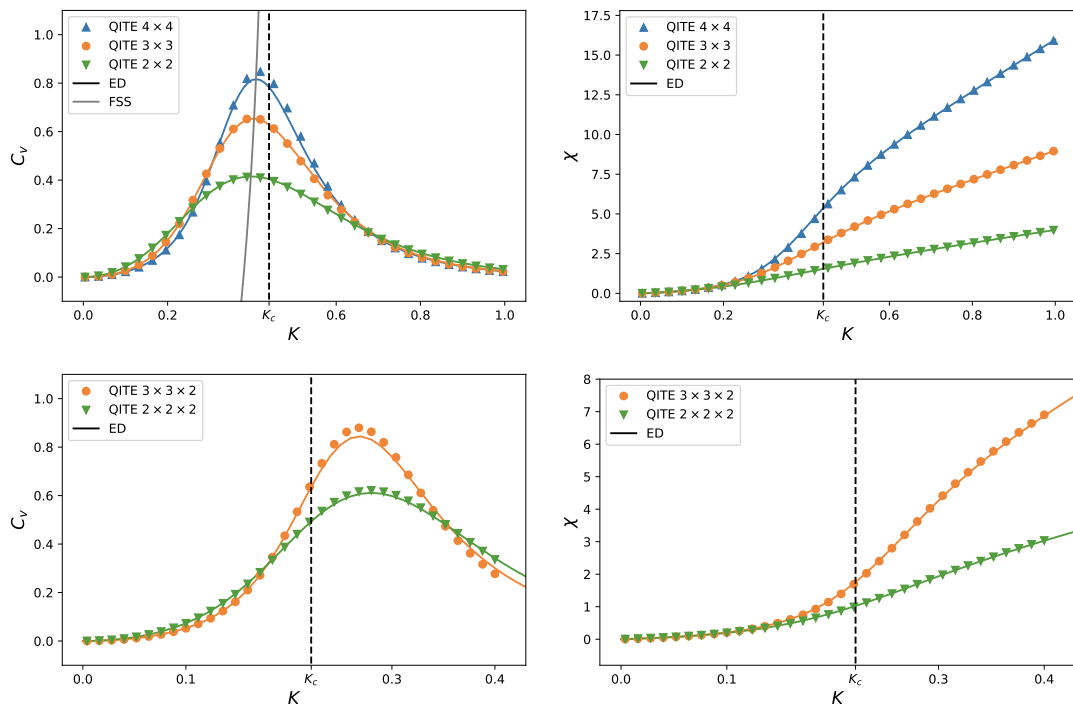


Figure 3. Specific heat(left column) and susceptibility(right column) as a function of K in 2-D(upper row) and 3-D(lower row) nearest-neighbor Ising model($\alpha = \infty$). ED represents results from exact diagonalization. We see that the results from the noiseless quantum simulation are close to exact diagonalization, especially in the region far from the critical point. The black dashed lines in the four panels are the exact critical temperatures K_c of the corresponding dimension in the infinite volume limit. The solid grey line in the upper left panel shows the peak movement as the system size enlarged, which is fitted inspired by finite size scaling (FSS). As the lattice size increases, the peaks of the specific heat and the leaps of the susceptibility are more obvious, and the transition points approach the exact critical point.

expressivity can be improved by increasing the number of ansatz layers and using longer Pauli strings for each local interaction term beyond $Z_i Y_j, Y_i Z_j$. More detailed error analyses are shown in Appendix B.

Indications of the Ising criticality can be observed in figure 3. The critical temperatures of 2-D and 3-D systems in the infinite volume limit are denoted by the black dashed line. Near the critical points, values of the specific heat and susceptibility increase, and there are peaks in the specific heat as a function of K . For 2-D NNIM with volume $N_d \times N_d$, we denote the position of the peak as $K_c(N_d)$. For larger system sizes, $K_c(N_d)$ moves slowly towards the infinite volume critical point K_c . To guide the eye of this movement, we draw the grey solid line in the upper left panel of figure 3. The analytic expression of the grey solid line is inspired by the finite size scaling [?].

Figure 4 presents the behavior of the specific heat for the 2-D long-range interacting Ising model with finite α . Compared with the nearest neighbor interaction, the long-range model introduces more $Z_i Z_j$ interactions and requires more variational parameters. There are $N = |\Lambda|(|\Lambda| - 1)L$ parameters in the variational ansatz. The system size in the figure is $|\Lambda| = 3 \times 3$, with $\alpha = 1, 2, 3$ and the nearest neighbor case $\alpha = \infty$,

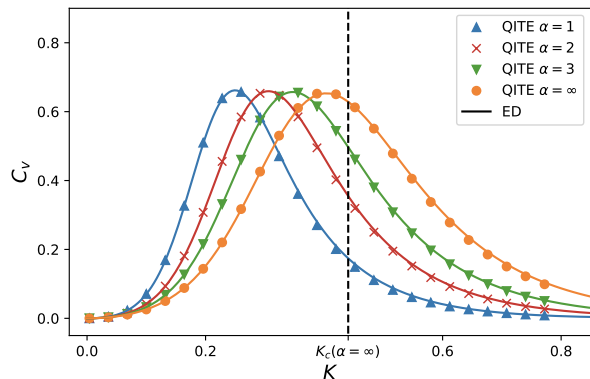


Figure 4. Specific heat as a function of K in the 2-D long-range interacting Ising model with interaction range $\alpha = 1, 2, 3, \infty$, where smaller α indicates larger interaction range. The system size is $|\Lambda| = 3 \times 3$. ED represents results from exact diagonalization. We see that for various α and K , the QITE results and the ED results are consistent. The black dashed line denotes the exact critical point of the 2-D NNIM in the infinite volume limit. As α decreases, the peak of the specific heat curve left shift, indicating that the effective dimension is raised for a larger interaction range.

marked by the triangular-up, cross, triangular-down and circle, respectively. We see that for various α and K , the QITE-ansatz results and the ED results are consistent. Moreover, the peak of the specific heat shifts to the direction of high temperature (smaller K) for a larger interaction range (smaller α). This behavior is reasonable since the long-range interaction effectively raises the system's dimension, and a higher system dimension leads to a higher critical temperature, e.g., 3-D NNIM critical temperature is higher than that of 2-D NNIM.

V. DISCUSSION

This work discusses the possibility of using the imaginary time evolution algorithm to prepare the thermal state of the Ising model on NISQ devices. We numerically calculate the specific heat and susceptibility of the long-range interacting Ising model with the prepared thermal state. We find that the results using the quantum algorithm are consistent with the ones from exact diagonalization for various temperatures, including the critical and low-temperature regions.

We present a systematic procedure to design a variational ansatz for the thermal state preparation. This ansatz is inherited from the quantum circuits used in QITE-measure algorithm. We show that it out-performs the original circuit designed using QITE-measure. This variational ansatz can be further simplified according to the symmetries of the Hamiltonian and the initial state.

In our numerical simulation results, indication of critical behavior can be observed in the calculation of heat capacity and susceptibility of 2-D and 3-D Ising model. The universality properties of Ising model including the critical exponents can be extracted from these quantities in the thermal dynamic limit, where larger Ising system should be simulated to approach the limit. Larger Ising system simulations resort to more advanced quantum devices with more qubits and less error, which are hopefully to be experimentally realized in the near future.

The ideas proposed in this work can be applied to study the critical behavior of other classical models, such as the Q -state Potts model, which would be difficult to simulate using the Monte-Carlo algorithm when Q is very large. Additionally, according to the correspondence of the D dimensional quantum model to the $D + 1$ dimensional classical model [34], the algorithm can also be used to study quantum phase transition.

VI. ACKNOWLEDGEMENTS

We thank Xiao Yuan, Jinzhao Sun, Lena Funcke, Stefan Kühn and Yahui Chai for helpful discussions. X.W. and X.F. were supported in part by NSFC of China under Grants No. 12125501, No. 12070131001, and No. 12141501, and National Key Research and Development

Program of China under No. 2020YFA0406400. PS acknowledges support from: ERC AdG NOQIA; Ministerio de Ciencia y Innovation Agencia Estatal de Investigaciones (PGC2018-097027-B-I00/10.13039/501100011033, CEX2019-000910-S/10.13039/501100011033, Plan National FIDEUA PID2019-106901GB-I00, FPI, QUANTERA MAQS PCI2019-111828-2, QUANTERA DYNAMITE PCI2022-132919, Proyectos de I+D+I “Retos Colaboración” QUSPIN RTC2019-007196-7); MICIIN with funding from European Union NextGenerationEU (PRTR-C17.I1) and by Generalitat de Catalunya; Fundació Cellex; Fundació Mir-Puig; Generalitat de Catalunya (European Social Fund FEDER and CERCA program, AGAUR Grant No. 2021 SGR 01452, QuantumCAT U16-011424, co-funded by ERDF Operational Program of Catalonia 2014-2020); Barcelona Supercomputing Center MareNostrum (FI-2022-1-0042); EU Horizon 2020 FET-OPEN OPTologic (Grant No 899794); EU Horizon Europe Program (Grant Agreement 101080086 — NeQST), National Science Centre, Poland (Symfonia Grant No. 2016/20/W/ST4/00314); ICFO Internal “QuantumGaudi” project; European Union’s Horizon 2020 research and innovation program under the Marie-Sklodowska-Curie grant agreement No 101029393 (STREDCH) and No 847648 (“La Caixa” Junior Leaders fellowships ID100010434: LCF/BQ/PI19/11690013, LCF/BQ/PI20/11760031, LCF/BQ/PR20/11770012, LCF/BQ/PR21/11840013). Views and opinions expressed in this work are, however, those of the author(s) only and do not necessarily reflect those of the European Union, European Climate, Infrastructure and Environment Executive Agency (CINEA), nor any other granting authority. Neither the European Union nor any granting authority can be held responsible for them.

Appendix A: Simplification of thermal state preparation in classical field theory

The Hamiltonian of a classical field theory is naturally diagonalized and can be written as a linear combination of Pauli- Z operators, such as the Ising model considered in the main text and Q -state Potts model. Such Hamiltonian has energy eigenstates that can be encoded on the computational basis of qubits, and all the Pauli- Z operators commute with each other. To compute the expectation values of such Hamiltonian’s thermal state, we only need imaginary time evolution on an initial state $|\bar{\pm}\rangle \equiv |+\rangle^{\otimes N_q}$ where N_q is the number of system’s qubits and $|+\rangle = (|0\rangle + |1\rangle)/\sqrt{2}$. A similar idea is also proposed in the tensor network algorithm targeting on classical Ising model [35]. The above statement is proved as follows.

The thermal expectation values $\langle O \rangle$ as defined in Eq. (4) can be expanded with an arbitrary orthogonal

basis $\{|i\rangle\}$

$$\langle O \rangle = \frac{\sum_i \langle i | e^{-\tau H} O e^{-\tau H} | i \rangle}{Z_{2\tau}}, \quad (\text{A1})$$

where

$$Z_{2\tau} = \sum_i \langle i | e^{-2\tau H} | i \rangle. \quad (\text{A2})$$

We choose the orthogonal basis of Pauli- X operators $\{|i\rangle\} = \{|+\rangle, |-\rangle\}^{\otimes N_q}$. Notice that all vectors in the set can be generated by applying Pauli- Z operators on one basis vector $|\tilde{+}\rangle$. For example

$$Z_2 Z_1 |+\rangle_2 |+\rangle_1 |+\rangle_0 = |-\rangle_2 |-\rangle_1 |+\rangle_0. \quad (\text{A3})$$

The Hamiltonian consists of Pauli- Z operators, so it commutes with all the Pauli- Z operators. Thus, all terms in the partition function are equal

$$\langle i | e^{-2\tau H} | i \rangle = \langle \tilde{+} | e^{-2\tau H} | \tilde{+} \rangle, \quad (\text{A4})$$

for all $|i\rangle \in \{|+\rangle, |-\rangle\}^{\otimes N_q}$, and we have $Z_{2\tau} = 2^{N_q} \langle \tilde{+} | e^{-2\tau H} | \tilde{+} \rangle$. Further, notice that all the observables concerning specific heat and susceptibility in Eq. (8) consist of Pauli- Z operators, which can be formally written as

$$O = \sum_m h_m \tilde{Z}_m, \quad (\text{A5})$$

where \tilde{Z}_m denotes the tensor product of Z operators at some sites and identity operators at others. Similar to Eq. (A4), all terms in the numerator of Eq. (A1) are equal

$$\langle i | e^{-\tau H} \tilde{Z}_m e^{-\tau H} | i \rangle = \langle \tilde{+} | e^{-\tau H} \tilde{Z}_m e^{-\tau H} | \tilde{+} \rangle, \quad (\text{A6})$$

for all $|i\rangle \in \{|+\rangle, |-\rangle\}^{\otimes N_q}$. Thus we have

$$\begin{aligned} \langle \tilde{Z}_m \rangle &= \frac{2^{N_q} \langle \tilde{+} | e^{-\tau H} \tilde{Z}_m e^{-\tau H} | \tilde{+} \rangle}{Z_{2\tau}} \\ &= \frac{\langle \tilde{+} | e^{-\tau H} \tilde{Z}_m e^{-\tau H} | \tilde{+} \rangle}{\langle \tilde{+} | e^{-2\tau H} | \tilde{+} \rangle}. \end{aligned} \quad (\text{A7})$$

In conclusion, the thermal expectation value of an observable $O = \sum_m h_m \tilde{Z}_m$ with a thermal state of a classical Hamiltonian can be derived according to imaginary time evolution on initial state $|\tilde{+}\rangle$,

$$\begin{aligned} \langle O \rangle &= \sum_m h_m \langle \tilde{Z}_m \rangle \\ &= \sum_m h_m \frac{\langle \tilde{+} | e^{-\tau H} \tilde{Z}_m e^{-\tau H} | \tilde{+} \rangle}{\langle \tilde{+} | e^{-2\tau H} | \tilde{+} \rangle} \\ &= \sum_m h_m \langle \tilde{+}(\tau) | \tilde{Z}_m | \tilde{+}(\tau) \rangle, \end{aligned} \quad (\text{A8})$$

where $|\tilde{+}(\tau)\rangle$ is imaginary time evolved state according to Eq. (9). The state is initialized as $|\tilde{+}(0)\rangle = |\tilde{+}\rangle$. Thus we prove the statement in Eq. (26).

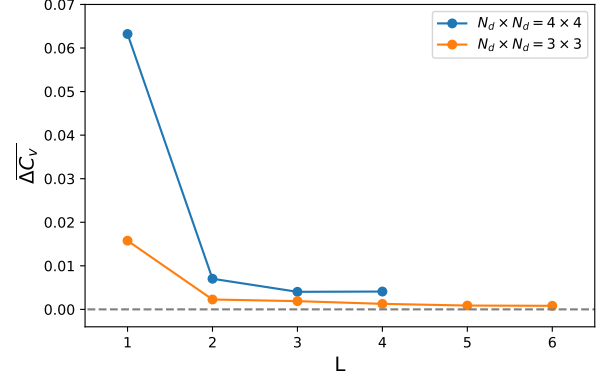


Figure 5. The average absolute error of specific heat as a function of variational ansatz layers. We utilize the 2-D nearest neighbor Ising model with two volumes $|\Lambda| = N_d \times N_d = 3 \times 3, 4 \times 4$. The limitation of variational ansatz can be well controlled by increasing the layers. As the number of layers is larger than some transition layers L^* , the error has no obvious change. Theoretically, we can predict $L^* \in [1.5, 3]$ for $N_d = 3$ and $L^* \in [2, 4]$ for $N_d = 4$.

Appendix B: Error analysis and circuit layers estimation

There are four main sources of errors when implementing the QITE-ansatz algorithm on real quantum devices [36]

- The variational ansatz has limited expressivity. The imaginary time evolution proceeds on the manifold expanded by the variational ansatz. Thus the evolved wave function deviates from the true wave function in Eq. (9), and leads to the systematic error of the expectation values of the observables.
- Errors arise from the numerical integration using the Euler method as in Eq. (19).
- Noisy quantum gates and readout processes in quantum devices result in systematic errors when evaluating expectation values and estimating M and V (See Eq. (17)).
- Finite number of shots results in statistical errors in evaluating expectation values, M and V .

Errors from the first and the second items are specific to the QITE-ansatz algorithm. The third and fourth errors exist in general for any quantum algorithms. In the following contents, we will discuss these errors in detail.

The errors from the limited variational ansatz expressivity have been shortly discussed in the main text. There are two ways to improve expressivity. The first is by increasing the number of ansatz layers, and the second is by considering longer Pauli strings expansion in Eq. (29) for each local interaction term in the Hamiltonian. It is not hard to see that by extending number of layers to

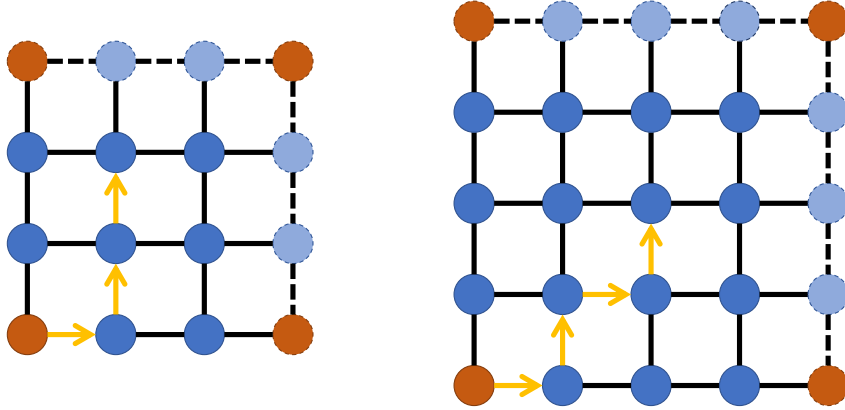


Figure 6. An Illustration to explain the transition layer in figure 5. We plot the 2-D nearest neighbor Ising model with two volumes $|\Lambda| = 3 \times 3, 4 \times 4$. Circles with solid edges are real spins. Circles with dashed edges are virtual spins from the periodic boundary condition. The spin at the origin(lower left corner) is denoted by the orange circle, which has three corresponding dashed-edge circles at three other corners. The yellow arrows denote the shortest path connecting the most remote spin to the spin at the origin. One layer of the variational ansatz generates the correlation between two spins at least 1 unit length apart. With at most $DN_d/2$ layers, the variational ansatz can connect all the spins in the graph.

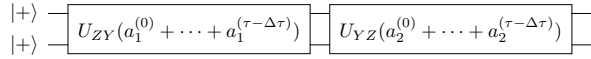


Figure 7. The quantum circuit equivalent to the QITE-measure circuit in figure 2a. Here $U_{ZY}(\theta) \equiv e^{-i\theta ZY}$, $U_{YZ}(\theta) \equiv e^{-i\theta YZ}$. This circuit can be expressed perfectly with only one layer of the variational ansatz in figure 2b.

infinity and taking the expansion on the whole system, the variational ansatz can carry out the evolution $e^{-\tau H}$ exactly. In the following text, we numerically investigate how these two aspects affect the performance in calculating the specific heat of 2-D NNIM.

The limitation of finite ansatz layers can be observed by tuning the number of layers L . In figure 5, we compute the average absolute error of 2-D NNIM specific heat as a function of L , in case of lattice volumes $|\Lambda| = 3 \times 3, 4 \times 4$. The average absolute error is defined by

$$\overline{\Delta C_v} \equiv \frac{1}{|K_{\max} - K_{\min}|} \int_{K_{\min}}^{K_{\max}} dK |C_v - C_v^{ED}|, \quad (\text{B1})$$

where C_v is specific heat from the quantum simulator, and C_v^{ED} is from exact diagonalization. Here we take the integration range $[K_{\min}, K_{\max}] = [0, 1]$. The errors of specific heat decrease rapidly as L increase and saturate to a platform after a certain layer L^* . We will analyze this transition layers L^* after a while. When $L > L^*$,

the remaining average absolute error of specific heat is mainly from the finite length of Pauli strings expansion.

Here provide an empirical explanation of the transition layer L^* , as observed in figure 5. It also helps to estimate how many layers we need when constructing variational ansatz for simulating NNIM. As shown in figure 6, variational ansatz generates correlation in the spin system. In the best case, the correlation between two neighboring spins is generated by one unitary transformation such as $e^{-i\theta ZY}$ in the Ising case; In the worst case, we need a whole layer of the variational ansatz such as $e^{-i\theta ZY} e^{-i\theta' YZ}$ to generate such correlation. The transition layer L^* indicates the lowest number of circuit layers to generate correlation between the two most distant spins in the D-dimensional nearest neighbor lattice system. Thus for D-dimensional NNIM with volume N_d^D and PBC, as the Manhattan distance of the most remote two spins is $DN_d/2$ (Equal to the number of the yellow arrows in figure 6, where $D = 2, N_d = 3, 4$ respectively.), the transition layer would be in the range

$$\frac{DN_d}{2G} \leq L^* \leq \frac{DN_d}{2}, \quad (\text{B2})$$

which corresponds to the best case and worst case mentioned above. Here G is the number of Pauli exponentials in one layer, i.e., the number of relevant Pauli operators for some local interaction terms. The transition layers in figure 5 are in accord with this range, i.e., $N_d/2 \leq L^* \leq N_d$, and we see larger number of layers have almost no improvement to the average absolute error of

the specific heat. Thus we say L^* layers are enough for variational ansatz to simulate NNIM. This estimation on the number of ansatz layers can be generalized to more complicated short-range interacting models.

Comparing the required number of layers of the variational ansatz provided by Eq. (B2) and the layers of quantum circuits used in QITE-measure, one finds the former is much less than the latter. It can be partially explained using the example of the two-qubit Ising system shown in the main text. For the QITE-measure circuit figure 2a, due to the commutability of relevant Pauli operators $[ZY, YZ] = 0$, it is equivalent to the circuit shown in figure 7, which consists of only two Pauli exponentials where the rotation angles are the summation of all the coefficients of the corresponding Pauli exponentials in figure 2a. Therefore, if we use one layer of the circuit in figure 2b, and $\theta_1 = a_1^{(0)} + \dots + a_1^{(\tau-\Delta\tau)}$, $\theta'_1 = a_2^{(0)} + \dots + a_2^{(\tau-\Delta\tau)}$, the QITE-measure circuit could be rephrased without loss of the precision. Thus compared with the QITE-measure circuit, the number of variational ansatz layers used in our simulation can be significantly reduced.

Numerical integration errors can be controlled via a more elaborate numerical integration algorithm. In the main text, we use the Euler method that accumulates a global error of $\mathcal{O}(\delta\tau)$ at the final step. One could use a more elaborate numerical algorithm such as the 4th-order Runge-Kutta method to control the systematic error, which accumulates a global error of $\mathcal{O}(\delta\tau^4)$ at the final step. In our simulations, as the numerical integration error is not the dominate systematic error, the Euler method is sufficiently good.

Errors from noisy quantum gates and readout processes lead to systematic deviations of the measurement results to the noiseless ones. For NISQ devices, there are many error mitigation techniques to reduce these deviations. For example, errors from two-qubit gates can be mitigated by zero-noise extrapolation [36, 37] and quasi-probability decomposition [36, 38]. The readout error can be mitigated by classical bit-flip correction [39, 40]. The error mitigation techniques reduce the systematic deviations of the noisy results to the noiseless ones and shed light on the real applications of NISQ devices [41, 42].

Finite number of shots error is a statistical error, which can be suppressed by increasing the number of shots. In the measurement procedure, the observables are split into a weighted sum of Pauli operators and each can be measured separately, at the cost of many shots. The number of shots can be reduced by collecting mutually commuting Pauli operators together before measuring all operators within a collection simultaneously [43, 44]. In the measurement process of the Ising model in Figure 1, the weighted Pauli operators are mutually commuting Pauli-Z strings. They can be measured simultaneously in computational basis.

Appendix C: Execution time of the nearest-neighbor Ising model

In this appendix, we estimate the execution time to study the critical behavior of the nearest-neighbor Ising model (NNIM) using the QITE-ansatz algorithm.

The execution time of the QITE-ansatz algorithm can be estimated by the number of steps of the imaginary time evolution, times the number of expectation values evaluated per step, times the number of two-qubit quantum gates (Assume no parallelization of the quantum gates, and the two-qubit gates dominate the execution time), i.e.,

$$\text{time} \sim (\text{steps}) \times (\# \text{ of expectations}) \times (\# \text{ of gates}). \quad (\text{C1})$$

Among the three factors, if the critical temperature of the system is of $\mathcal{O}(1)$, then the total evolution should have the same order, and the number of evolution steps is a constant, which is the case of simulating NNIM.

For each step of the time evolution, one needs to estimate the expectation values of entries of the M matrix and V vector. Thus

$$\# \text{ of expectations} \sim \mathcal{O}(N^2), \quad (\text{C2})$$

where N is the dimension of the M matrix, equals the number of variational parameters. For the variational ansatz proposed in this work, the number of variational parameters is $N = 2D|\Lambda|L$ for NNIM, where D is the spatial dimension of the NNIM lattice Λ , $|\Lambda|$ is the lattice size, L is the number of ansatz layers. In Appendix B of the manuscript, we estimate the number of layers required for NNIM, where $L \sim \mathcal{O}(DN_d)$, N_d is the side length of Λ . The lattice size and the side length are related by $|\Lambda| = N_d^D$. Thus, the number of expectation evaluations reads

$$\# \text{ of expectations} \sim \mathcal{O}(D^4 N_d^{2D+2}). \quad (\text{C3})$$

To count the number of two-qubit quantum gates, we assume that the CNOT gate is the basic two-qubit gate that can be realized on quantum devices, and the CNOT gate can be applied to every two-qubit pair. Then, the number of CNOT gates in the proposed ansatz is proportional to its number of variational parameters N , so that

$$\# \text{ of gates} \sim \mathcal{O}(D^2 N_d^{D+1}). \quad (\text{C4})$$

In summary, the execution time of the QITE-ansatz algorithm for D-dimensional NNIM reads

$$\text{time} \sim \mathcal{O}(D^6 N_d^{3D+3}), \quad (\text{C5})$$

which is a polynomial function of the system size.

There are some improvement methods of the QITE-ansatz algorithm to reduce the execution time, such as

the DualQITE algorithm proposed in reference [45]. Using this algorithm, one can reduce the number of expectation evaluations in Eq. (C2) from $\mathcal{O}(N^2)$ to $\mathcal{O}(N)$, and

the total execution time is correspondingly reduced to

$$\text{time} \sim \mathcal{O}(D^4 N_d^{2D+2}). \quad (\text{C6})$$

-
- [1] Sam McArdle, Suguru Endo, Alán Aspuru-Guzik, Simon C. Benjamin, and Xiao Yuan. Quantum computational chemistry. *Rev. Mod. Phys.*, 92:015003, Mar 2020.
- [2] N. Klco, E. F. Dumitrescu, A. J. McCaskey, T. D. Morris, R. C. Pooser, M. Sanz, E. Solano, P. Lougovski, and M. J. Savage. Quantum-classical computation of schwinger model dynamics using quantum computers. *Phys. Rev. A*, 98:032331, Sep 2018.
- [3] Natalie Klco, Martin J. Savage, and Jesse R. Stryker. $Su(2)$ non-abelian gauge field theory in one dimension on digital quantum computers. *Phys. Rev. D*, 101:074512, Apr 2020.
- [4] Anthony Ciavarella, Natalie Klco, and Martin J. Savage. Trailhead for quantum simulation of $su(3)$ yang-mills lattice gauge theory in the local multiplet basis. *Phys. Rev. D*, 103:094501, May 2021.
- [5] L. Funcke, T. Hartung, K. Jansen, S. Kühn, M. Schneider, P. Stornati, and X. Wang. Towards quantum simulations in particle physics and beyond on noisy intermediate-scale quantum devices. *Philosophical Transactions of the Royal Society A: Mathematical, Physical and Engineering Sciences*, 380(2216), Feb 2022.
- [6] Giuseppe Clemente, Arianna Crippa, and Karl Jansen. Strategies for the determination of the running coupling of $(2 + 1)$ -dimensional qed with quantum computing, 2022.
- [7] Simulating lattice gauge theories within quantum technologies. *The European Physical Journal D*, 74(8):165, 2020.
- [8] Barbara M. Terhal and David P. DiVincenzo. Problem of equilibration and the computation of correlation functions on a quantum computer. *Phys. Rev. A*, 61:022301, Jan 2000.
- [9] Jingxiang Wu and Timothy H. Hsieh. Variational thermal quantum simulation via thermofield double states. *Phys. Rev. Lett.*, 123:220502, Nov 2019.
- [10] R. Sagastizabal, S. P. Premaratne, B. A. Klaver, M. A. Rol, V. Negîrneac, M. S. Moreira, X. Zou, S. Johri, N. Muthusubramanian, M. Beekman, C. Zachariadis, V. P. Ostroukh, N. Haider, A. Bruno, A. Y. Matsuura, and L. DiCarlo. Variational preparation of finite-temperature states on a quantum computer. *npj Quantum Information*, 7(1):130, 2021.
- [11] Anirban Narayan Chowdhury and Rolando D. Somma. Quantum algorithms for gibbs sampling and hitting-time estimation. *Quantum Info. Comput.*, 17(1-2):41-64, feb 2017.
- [12] Sam McArdle, Tyson Jones, Suguru Endo, Ying Li, Simon C. Benjamin, and Xiao Yuan. Variational ansatz-based quantum simulation of imaginary time evolution. *npj Quantum Information*, 5(1):75, 2019.
- [13] Mario Motta, Chong Sun, Adrian T. K. Tan, Matthew J. O’Rourke, Erika Ye, Austin J. Minnich, Fernando G. S. L. Brandão, and Garnet Kin-Lic Chan. Determining eigenstates and thermal states on a quantum computer using quantum imaginary time evolution. *Nature Physics*, 16(2):205-210, 2020.
- [14] Marcello Benedetti, Mattia Fiorentini, and Michael Lubasch. Hardware-efficient variational quantum algorithms for time evolution. *Phys. Rev. Res.*, 3:033083, Jul 2021.
- [15] John Preskill. Quantum computing in the NISQ era and beyond. *Quantum*, 2:79, aug 2018.
- [16] Kishor Bharti, Alba Cervera-Lierta, Thi Ha Kyaw, Tobias Haug, Sumner Alperin-Lea, Abhinav Anand, Matthias Degroote, Hermanni Heimonen, Jakob S. Kottmann, Tim Menke, Wai-Keong Mok, Sukin Sim, Leong-Chuan Kwek, and Alán Aspuru-Guzik. Noisy intermediate-scale quantum algorithms. *Rev. Mod. Phys.*, 94:015004, Feb 2022.
- [17] Junyu Liu, Jinzhao Sun, and Xiao Yuan. Towards a variational jordan-lee-preskill quantum algorithm, 2021.
- [18] Christa Zoufal, Aurélien Lucchi, and Stefan Woerner. Variational quantum boltzmann machines. *Quantum Machine Intelligence*, 3(1), feb 2021.
- [19] R. Islam, C. Senko, W. C. Campbell, S. Korenblit, J. Smith, A. Lee, E. E. Edwards, C.-C. J. Wang, J. K. Freericks, and C. Monroe. Emergence and frustration of magnetism with variable-range interactions in a quantum simulator. *Science*, 340(6132):583-587, 2013.
- [20] Fangli Liu, Rex Lundgren, Paraj Titum, Guido Pagano, Jiehang Zhang, Christopher Monroe, and Alexey V. Gorshkov. Confined quasiparticle dynamics in long-range interacting quantum spin chains. *Phys. Rev. Lett.*, 122:150601, Apr 2019.
- [21] Joseph Vovrosh, Rick Mukherjee, Alvis Bastianello, and Johannes Knolle. Dynamical hadron formation in long-range interacting quantum spin chains, 2022.
- [22] We have also tried non-QITE-based variational quantum algorithm proposed in reference [9, 10]. We find its accuracy is not as good as the QITE-ansatz algorithm when the simulation is performed on a noiseless statevector quantum simulator.
- [23] Here we abuse bra-ket notation for the mixed state. It will be explained in detail in the subsection (III A).
- [24] Xiao Yuan, Suguru Endo, Qi Zhao, Ying Li, and Simon C. Benjamin. Theory of variational quantum simulation. *Quantum*, 3:191, oct 2019.
- [25] Lena Funcke, Tobias Hartung, Karl Jansen, Stefan Kühn, and Paolo Stornati. Dimensional Expressivity Analysis of Parametric Quantum Circuits. *Quantum*, 5:422, March 2021.
- [26] Steven R. White. Minimally entangled typical quantum states at finite temperature. *Phys. Rev. Lett.*, 102:190601, May 2009.
- [27] E M Stoudenmire and Steven R White. Minimally entangled typical thermal state algorithms. *New Journal of Physics*, 12(5):055026, may 2010.
- [28] Oliver Cole. Quantum circuit optimisation through stabiliser reduction of pauli exponentials, 2022.

- [29] M. A. Nielsen and I. L. Chuang. *Quantum Computation and Quantum Information*. Cambridge University Press, Cambridge, 2000.
- [30] Kübra Yeter-Aydeniz, Raphael C. Pooser, and George Siopsis. Practical quantum computation of chemical and nuclear energy levels using quantum imaginary time evolution and lanczos algorithms. *npj Quantum Information*, 6(1):63, 2020.
- [31] Héctor Abraham *et al.* Qiskit: An open-source framework for quantum computing, 2019.
- [32] T. D. SCHULTZ, D. C. MATTIS, and E. H. LIEB. Two-dimensional ising model as a soluble problem of many fermions. *Rev. Mod. Phys.*, 36:856–871, Jul 1964.
- [33] A F Sonsin, M R Cortes, D R Nunes, J V Gomes, and R S Costa. Computational analysis of 3d ising model using metropolis algorithms. *Journal of Physics: Conference Series*, 630:012057, jul 2015.
- [34] Timothy H. Hsieh. From d-dimensional quantum to d+1-dimensional classical systems. 2012.
- [35] F. Verstraete, M. M. Wolf, D. Perez-Garcia, and J. I. Cirac. Criticality, the area law, and the computational power of projected entangled pair states. *Phys. Rev. Lett.*, 96:220601, Jun 2006.
- [36] Ying Li and Simon C. Benjamin. Efficient variational quantum simulator incorporating active error minimization. *Phys. Rev. X*, 7:021050, Jun 2017.
- [37] Kristan Temme, Sergey Bravyi, and Jay M. Gambetta. Error mitigation for short-depth quantum circuits. *Phys. Rev. Lett.*, 119:180509, Nov 2017.
- [38] Suguru Endo, Simon C. Benjamin, and Ying Li. Practical quantum error mitigation for near-future applications. *Phys. Rev. X*, 8:031027, Jul 2018.
- [39] Lena Funcke, Tobias Hartung, Karl Jansen, Stefan Kühn, Paolo Stornati, and Xiaoyang Wang. Measurement error mitigation in quantum computers through classical bit-flip correction. *Phys. Rev. A*, 105:062404, Jun 2022.
- [40] Ewout van den Berg, Zlatko K. Mineev, and Kristan Temme. Model-free readout-error mitigation for quantum expectation values. *Phys. Rev. A*, 105:032620, Mar 2022.
- [41] Youngseok Kim, Andrew Eddins, Sajant Anand, Ken Xuan Wei, Ewout van den Berg, Sami Rosenblatt, Hasan Nayfeh, Yantao Wu, Michael Zaletel, Kristan Temme, and Abhinav Kandala. Evidence for the utility of quantum computing before fault tolerance. *Nature*, 618(7965):500–505, 2023.
- [42] Sirui Cao, Bujiao Wu, Fusheng Chen, Ming Gong, Yulin Wu, Yangsen Ye, Chen Zha, Haoran Qian, Chong Ying, Shaojun Guo, Qingling Zhu, He-Liang Huang, Youwei Zhao, Shaowei Li, Shiyu Wang, Jiale Yu, Daojin Fan, Dachao Wu, Hong Su, Hui Deng, Hao Rong, Yuan Li, Kaili Zhang, Tung-Hsun Chung, Futian Liang, Jin Lin, Yu Xu, Lihua Sun, Cheng Guo, Na Li, Yong-Heng Huo, Cheng-Zhi Peng, Chao-Yang Lu, Xiao Yuan, Xiaobo Zhu, and Jian-Wei Pan. Generation of genuine entanglement up to 51 superconducting qubits. *Nature*, 2023.
- [43] A. Kandala, A. Mezzacapo, K. Temme, et al. Hardware-efficient variational quantum eigensolver for small molecules and quantum magnets. *Nat.*, 549:242, 2017.
- [44] Ophelia Crawford, Barnaby van Straaten, Daochen Wang, Thomas Parks, Earl Campbell, and Stephen Brierley. Efficient quantum measurement of Pauli operators in the presence of finite sampling error. *Quantum*, 5:385, January 2021.
- [45] Julien Gacon, Jannes Nys, Riccardo Rossi, Stefan Woerner, and Giuseppe Carleo. Variational quantum time evolution without the quantum geometric tensor, 2023.